AIChE J., **24**, 709 (1978).
13. R. D. Armstrong, O. R. Brown, R. D. Giles, and J. A. Harrison, *Nature (London)*, **219**, 94 (1968).
14. O. Levenspiel, "Chemical Reaction Engineering," John Wiley, New York (1962).
15. V. Specchia and G. Baldi, *Chem. Eng. Sci.*, **32**, 515 (1977).
16. G. H. Neale and W. K. Nader, *AIChE J.*, **19**, 112 (1973).
17. C. Oloman and A. P. Watkinson, *J. Appl. Electrochem.*, **9**, 117 (1979).
18. C. Oloman, *This Journal*, **117**, 1604 (1970).
19. C. Oloman and A. P. Watkinson, U.S. Patent 4,118,-305 (1978).
20. S. Germain and F. Goodridge, *Electrochim. Acta.*, **21**, 545 (1976).
21. S. Ergun, *Chem. Eng. Prog.*, **48**, 89 (1952).
22. Y. Sato, T. Hirose, F. Takahashi, and M. Toda, *J. Chem. Eng. Jpn.*, **6**, 147 (1973).
23. M. L. Batia, M.A.Sc. Thesis, University of British Columbia (1978).
24. L. P. Reiss, *Ind. Eng. Chem. Process Des. Dev.*, **6**, 486 (1967).
25. E. J. Wilson and C. J. Geankopolis, *Ind. Eng. Chem. Fundam.*, **5**, 9 (1966).

Semiconductor Electrodes

XXI. The Characterization and Behavior of n-Type Fe_2O_3 Electrodes in Acetonitrile Solutions

Ronald A. Fredlein*,[1] and Allen J. Bard*

Department of Chemistry, The University of Texas at Austin, Austin, Texas 78712

ABSTRACT

The electrochemical behavior of Pb-doped single crystal, Ti-doped polycrystalline compacts, and chemical vapor deposited films of Fe_2O_3 was investigated in acetonitrile solutions. Details of the surface electronic band structure were obtained from capacitance and photo-excitation techniques and by comparing the cyclic voltammograms of various electroactive species of known standard potential to the Nernstian response at a Pt disk electrode. There is evidence that surface electronic states capable of mediating electron transfer exist at ~0.9 eV and ~1.8 eV negative of conduction bandedge. Results are interpreted in terms of a narrow conduction band of width dependent on the dopant level.

Recent interest in the semiconductor electrochemistry of Fe_2O_3 stems from the small bandgap (2.2 eV), n-type conduction, and stability in aqueous alkali that Fe_2O_3 possesses. This makes it an apparent attractive possible substrate for the photo-assisted decomposition of water (1-5) but quantum efficiencies are low (2-4). Less work has been done on its fundamental electrochemistry as dictated by its electronic band structure (6, 7). Intrinsic Fe_2O_3 is an excitation semiconductor of high resistivity (8) but when substitutionally doped by divalent (p-type) or tetravalent (n-type) cations, becomes conductive with charge transfer occurring by a thermally activated hopping mechanism (9-12). For example, a Ti^{4+} on a Fe^{3+} site is accommodated by the presence of a Fe^{2+} and conduction results from electron hopping between adjacent Fe^{2+} and Fe^{3+} ions. In this respect n-type Fe_2O_3 does not possess the usual wide conduction band composed of a continuum of delocalized electronic states. The electronic structure of α-Fe_2O_3 has been reviewed (13-15).

One of the more successful techniques for probing the surface electronic structure of semiconductor electrodes exploits the isoenergetic charge transfer between the semiconductor and donor/acceptor states in solution (16-18). The solution electronic states are provided by redox couples of known standard potential. Acetonitrile (ACN) is a preferred solvent for such studies because of its extended potential range of stability (~5V) and other previously documented reasons (18, 19). This paper reports studies of single crystal and polycrystalline compacts of α-Fe_2O_3 and chemical vapor deposited (CVD) films of approximate composition α (70%), ζ (20%), and γ (10%)-Fe_2O_3 (4).

* Electrochemical Society Active Member.
[1] Permanent address: Chemistry Department, University of Newcastle, N.S.W. 2308 Australia.
Key words: semiconductor, capacitance, voltammetry.

Experimental

Sintered polycrystalline compacts of α-Fe_2O_3 were prepared doped with titanium in the range 0.05-1.0 atomic percent (a/o) Ti. Fe_2O_3 (Fisher Certified) was stirred overnight with TiO_2 (MBC reagent grade) in acetone, the solvent evaporated and the powder pressed into disks at 7000 psi before firing in air at 1100°C for 16 hr (3, 10). Single crystals of α-Fe_2O_3, grown from a PbO melt, were generously donated by Sandia Laboratories. The black, lustrous crystals were highly conductive and on illumination gave rise to only negligibly small anodic photocurrents in 0.1M aqueous acetate buffer (pH 7.0) (1). However, heating the crystals in air at 540°C for 120 hr resulted in great enhancement of the photocurrents. The Pb content of the crystals was estimated to be in the 1-10 a/o range by x-ray fluorescence. The surfaces of the heat-treated and untreated crystals were examined by ESCA and Auger spectroscopy. Each crystal had one or two well-developed faces which were determined to be (012) (hexagonal indices) and the prepared electrodes exposed this face. Films of Fe_2O_3 on Pt foil were prepared by chemical vapor deposition (CVD) as previously described (1) and annealed for a few minutes in the oxidizing flame of a Fisher burner. A Cu wire contact was made to each electrode with conductive silver acrylic cement (Allied Products Corporation) the contacted surface of the sintered compacts and single crystals being first smeared with In/Ga alloy. The electrodes were mounted in glass tubes with silicone rubber sealant (Dow Corning) and studied without prior etching.

The preparation or purification of the anhydrous acetonitrile solvent, the tetra-n-butylammonium perchlorate (TBAP) electrolyte and the various electroactive reagents have been previously described (18, 20). For some reagents, controlled potential coulome-

try was used to transform them to the desired oxidation states.

A three compartment cell was used employing a silver quasi-reference electrode, the potential of which was periodically checked during each experiment against known standard potentials located by cyclic voltammetry at a Pt disk electrode (1). Experiments were performed in a He atmosphere (Vacuum Atmospheres Corporation, glove box); the ground joints of the cell were sealed with silicone vacuum grease if it was removed from the box.

Cyclic voltammograms were obtained using a PAR 173 potentiostat, PAR 175 function generator, and Houston Instruments Model 2000 X-Y recorder. Positive feedback was used to compensate for the *IR* drop in the solution and semiconductor. All the electrodes required about the same amount of feedback as that of the Pt disk except for the 0.05 a/o Ti electrodes, which required 20 times as much. Electrode capacitance measurements were made by superimposing a 5 mV sinusoidal signal (Wavetek VCG 114) on the steady-state electrode potential. The output signals from the current and voltage followers of the potentiostat were amplified and resolved into their in-phase and quadrature components (PAR 5204 lock-in amplifier) and measured with a DVM (Keithley 179). The capacitance and resistance were computed as series circuit elements.

For photoexcitation experiments, unfocused polychromatic radiation from a 250 W sunlamp was used to illuminate the electrode. The photocurrent-wavelength response was determined using a 450W Xenon lamp and Oriel 7240 monochromator (13 nm passband) and the data corrected for output variations of the source-monochromator.

Results

Dopant concentrations.—The surface dopant concentrations of the single crystals were determined by Auger spectroscopy to be 2.8 ± 0.5 and 0.8 ± 0.4 a/o Pb for untreated and heat-treated crystals, respectively These results are supported by ESCA data which show a 3.0:1 ratio of surface Pb for the same crystals.

Schottky-Mott plots.—In the potential region of the semiconductor depletion layer, the flatband potential, V_{fb}, and the donor density, N_D, can, in principle, be found from plots of C_{sc}^{-2} *vs.* V according to the Schottky-Mott equation

$$C_{sc}^{-2} = 2(V - V_{fb} - kT/e)/(e\epsilon\epsilon_0 N_D) \qquad [1]$$

where C_{sc} is the space charge region capacitance per unit area, ϵ the dielectric constant of the semiconductor, ϵ_0 the permittivity of free space and the other symbols have their usual meanings. In practice, frequency dispersion often results in uncertainties in the values of V_{fb} and N_D so obtained (21) as is illustrated by the present data, Fig. 1 and Tables I and II. In the calculation of N_D, the slopes of the low potential, linear region of the curves were used with ϵ taken as 120 and no attempt was made to correct for electrode roughness. These donor densities vary greatly

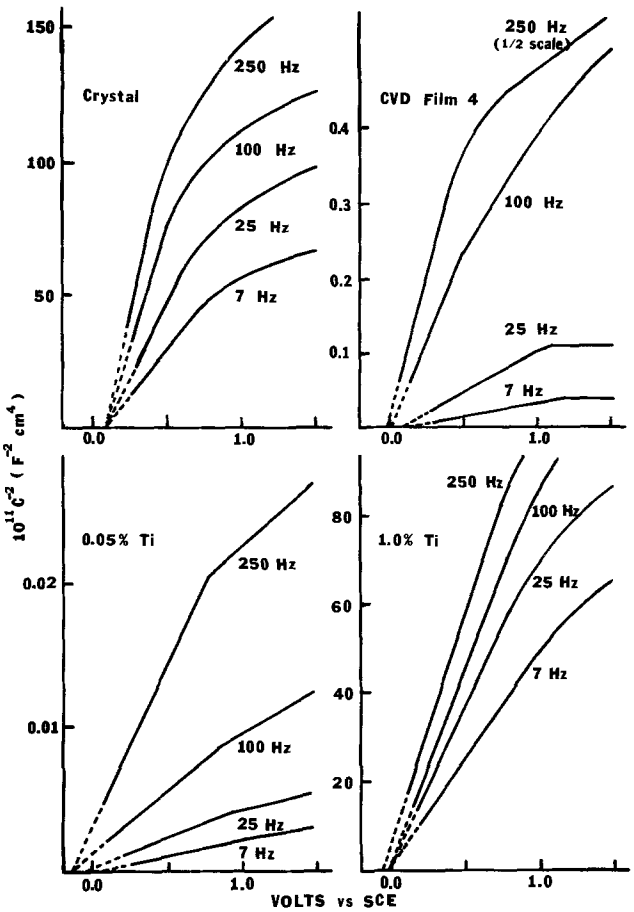

Fig. 1. Schottky-Mott plots for some Fe_2O_3 electrodes in 0.100M TBAP, ACN at various frequencies.

with frequency (Table I; Fig. 1). This type of frequency dispersion has been interpreted as due to a frequency dependent dielectric constant and N_D values can then be interpreted as having relative significance only (21, 22). The N_D values at lowest frequency (7 Hz) are considered the most appropriate as an aid to the interpretation of the essentially d-c cyclic voltammograms (vide infra). The N_D (7 Hz) value for the single crystal establishes that its effective donor density is near the top of the range studied. This is in agreement with the surface dopant concentrations and suggests that, like Ti, Pb occupies substitutional Fe sites and exists as Pb^{4+}. Similarly the empirical donor density of the CVD film electrodes is towards the bottom of the range and, since these electrodes exhibit the greatest frequency dispersion, their effective d-c donor density may be relatively lower.

Kennedy and Frese (3) have reported Schottky-Mott plots at 1000 Hz for polycrystalline sintered disks of α-Fe_2O_3 doped by 0-1.0 a/o Ti in contact with

Table I. Donor densities, N_D, determined from Schottky-Mott plots at various frequencies

Electrode	Dopant[a] (cm^{-3})	N_D (7 Hz) (cm^{-3})	N_D (25 Hz) (cm^{-3})	N_D (100 Hz) (cm^{-3})	N_D (250 Hz) (cm^{-3})
Crystal	3.2×10^{20}[b]	2.0×10^{19}	1.2×10^{19}	7.6×10^{18}	6.0×10^{18}
CVD film[c]	—	3.4×10^{18}	1.1×10^{18}	2.5×10^{17}	7.6×10^{16}
1.0% Ti	4.0×10^{20}	2.6×10^{19}	1.9×10^{19}	1.6×10^{19}	1.3×10^{19}
0.5% Ti	2.0×10^{20}	1.6×10^{19}	1.3×10^{19}	1.1×10^{19}	8.9×10^{18}
0.2% Ti	8.0×10^{19}	1.2×10^{19}	7.3×10^{18}	5.2×10^{18}	4.4×10^{18}
0.1% Ti	4.0×10^{19}	6.4×10^{18}	4.6×10^{18}	3.8×10^{18}	2.2×10^{18}
0.05% Ti	2.0×10^{19}	4.8×10^{17}	3.6×10^{17}	1.2×10^{17}	5.4×10^{16}

[a] Density taken at 5.2 g cm^{-3}.
[b] Surface density of Pb.
[c] CVD film No. F4.

Table II. Schottky-Mott flatband potentials compared to the potentials of onset of the photo-oxidation of N,N,N',N'-tetramethyl-p-phenylenediamine at various Fe_2O_3 electrodes

Electrode	V_{fb}[a] (V (SCE))	Onset potential (V (SCE))
Single crystal	0.06 ± 0.01	0.04
CVD film	−0.02 ± 0.02	−0.06
Compact 0.05% Ti	−0.06 ± 0.02	0.06
0.1% Ti	−0.05 ± 0.01	0.04
0.2% Ti	−0.05 ± 0.05	0.02
0.5% Ti	−0.01 ± 0.01	0.06
1.0% Ti	−0.12 ± 0.06	0.04

[a] V_{fb} given as the range of intercepts for frequencies of 7, 25, 100, and 250 Hz.

aqueous solutions. Their results for pure α-Fe_2O_3 are of the same form as the current results for 0.05 a/o Ti; both show breaks in the linear plots. Also at higher Ti concentrations, both sets of data give linear plots to ~1V positive of V_{fb}. However, Kennedy and Frese (3) found donor densities for the Ti-doped electrodes ~5 times those of the present study. Their higher N_D values may be due to quenching during the preparation of their sintered compacts which freezes in oxygen vacancies increasing N_D (9). The transition to a lower second slope exhibited by the low N_D value electrodes has been interpreted as due to deep donors in these and other materials (3, 23). We note that in the present study the potential of slope change is frequency dependent.

Photocurrents.—Photocurrents were always anodic and the photocurrent-wavelength response determined in 1.0 mM thianthrene (Th) at 1.5V (Fig. 2) was of the same form for all samples. The photocurrent den-

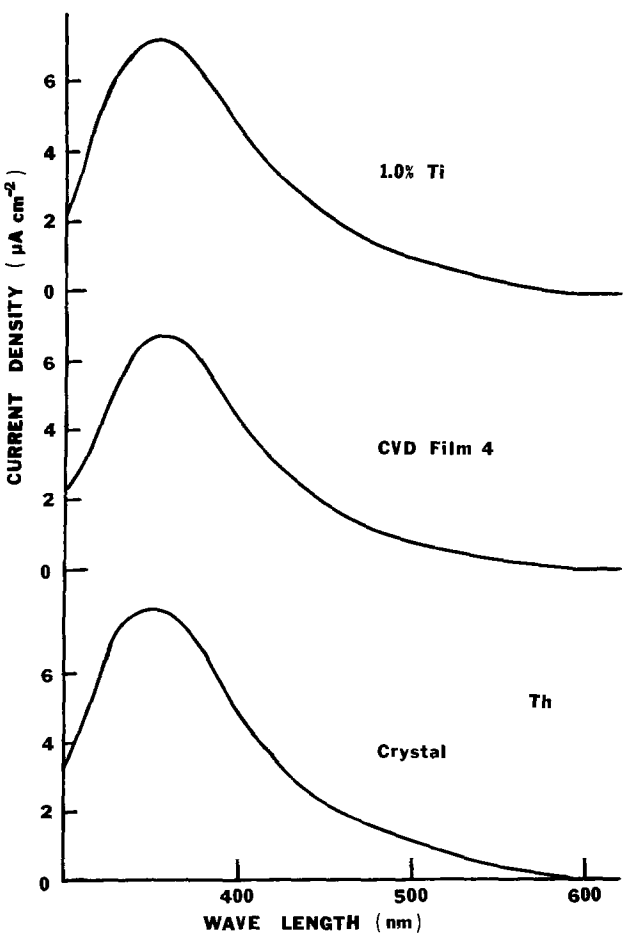

Fig. 2. Photocurrent-wavelength response for Fe_2O_3 electrodes corrected for output variations of the source/monochromator in 1.0 mM thianthrene, 0.100M TBAP, ACN at 1.5V.

Table III. Cyclic voltammetric peak potentials for various redox reactions at Pt and Fe_2O_3 electrodes in 0.1M TBAP in ACN

Redox reaction [a]	Pt		α-Fe_2O_3 crystal		Fe_2O_3 CVD film		α-Fe_2O_3 0.05% Ti		α-Fe_2O_3 0.1% Ti		α-Fe_2O_3 0.2% Ti		α-Fe_2O_3 0.5% Ti		α-Fe_2O_3 1.0% Ti	
	E_{pc}	E_{pa}	E_{pc}	E_{pa}	E_{pc}	E_{pa}	E_{pc}	E_{pa}	E_{pc}	E_{pa}	E_{pc}	E_{pa}	E_{pc}	E_{pa}	E_{pc}	E_{pa}
$AQ + e^- \rightleftarrows AQ^-$	−0.98	−0.91	−1.12	−0.72	−1.32	−0.68	−1.45	−0.61	−1.36	−0.62	−1.18	−0.70	−1.20	−0.67	−1.24	−0.66
$BQ + e^- \rightleftarrows BQ^-$	−0.56	−0.49	−0.92	−0.26	−1.47	−0.28	−1.35	[b]	−0.96	−0.08	−1.06	0.10	−0.89	−0.06	−0.91	−0.04
$BQ^- \rightleftarrows BQ + e^-$	−0.56	−0.49	−0.84	−0.26	−0.92	−0.28	−1.00	[b]	−0.90	−0.06	−0.86	0.08	−0.84	−0.02	−0.86	−0.04
$Ox\text{-}1^+ + e^- \rightleftarrows OX^\cdot$	−0.46	−0.39	−0.59	−0.26	−0.84	−0.20			−0.73	−0.06	−0.68	−0.02	−0.63	−0.18	−0.57	−0.23
$TMPD \rightleftarrows TMPD^{+\cdot} + e^-$	0.19	0.26	0.02	[b]	−0.04	[b]	−0.12	[b]	0.00	[b]	0.07	[b]	0.02	0.66	0.08	0.45
$10MP^{+\cdot} + e^- \rightleftarrows 10MP$	0.79	0.86	0.49		0.27		0.20		0.59	[b]			0.60	[b]	0.65	0.98
$Th^{+\cdot} + e^- \rightleftarrows Th$	1.20	1.26	0.83		[b]		0.67		0.87		0.89		0.82		0.87	
$R^{3+} + e^- \rightleftarrows R^{2+}$	1.27	1.33	0.87		[b]				0.85		0.95		0.90		1.00	

[a] Abbreviations: AQ, anthraquinone; BQ, p-benzoquinone; Ox-1$^+$, oxazine-1; TMPD, N,N,N',N'-tetramethyl-p-phenylenediamine; 10MP, 10-methylphenothiazine; Th, thianthrene; R^{2+}, $Ru(bipy)_3^{2+}$.
[b] Current flow but no distinct peak.

sity varied by a factor of 2 and exhibited no trend with N_D. The photocurrent first becomes detectable at 590 nm (E_g = 2.10 eV) and the maximum of the response corresponds to the minimum of reflectance spectrum (341 nm) (24). The photocurrent density rises only gently from its onset with increasingly energetic radiation (Fig. 2) indicating a very small extinction coefficient for the excitation process. Kennedy and Frese (6) have concluded that excitation, forming holes in the valence band, is an indirect process requiring phonon support. Small extinction coefficients are characteristic of such processes (25).

Under illumination, the photo-oxidations of N,N,N',N'-tetramethyl-p-phenylenediamine (TMPD), 10-methylphenothiazine (10-MP), Th, and $Ru(bipy)_3^{2+}$ were observed at potentials negative of their reversible potentials. Only in the absence of a dark current is it certain that illumination produces a photocurrent rather than convective enhancement of the dark current (26). The most negative potential of photo-oxidation, which occurred for TMPD on all electrodes, then corresponds to V_{fb} (Table III). Photocurrent measurements generally provide a more reliable determination of V_{fb} than do the X-axis intercepts of the Schottky-Mott plots (26) but for the present study, the agreement between the two sets of data is good (Table II) except for the CVD film. For this electrode the photocurrent onset potential is the more negative and therefore the preferred value.

Linear and cyclic voltammetry.—Figure 3 shows i against V scans, starting at 0V (SCE), in both the positive and negative directions and indicates the working ranges of the various Fe_2O_3 electrodes, compared to that of platinum, in 0.100*M* TBAP in ACN. All anodic currents are due to the oxidation of the electrolyte solution which probably involves

$$ClO_4^- \rightarrow ClO_4^{\cdot} + e^- \qquad ClO_4^{\cdot} \rightarrow ClO_2^{\cdot} + O_2 \qquad [2]$$

but, for the Fe_2O_3 electrodes, the cathodic currents correspond to the irreversible reduction of the substrate.

Cyclic voltammetry at the Fe_2O_3 electrodes was carried out for a number of compounds that undergo reversible, one-electron charge transfer processes at platinum and the results are summarized in Table III. These experiments were performed in the dark at scan rates of 50 or 100 mV sec^{-1} except where noted.

The standard potential of the $AQ/AQ^{\cdot -}$ couple is the most negative of any couple studied and is almost a volt below the flatband potentials. The cyclic voltammograms, Fig. 4, exhibit irreversible to quasi-reversible behavior with the peak separation decreasing

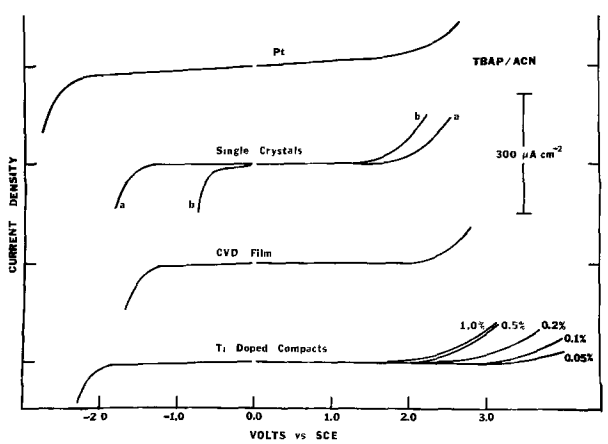

Fig. 3. Current density against potential curves for the electrodes in 0.100*M* TBAP, ACN; (a) heat-treated crystal; (b) untreated crystal.

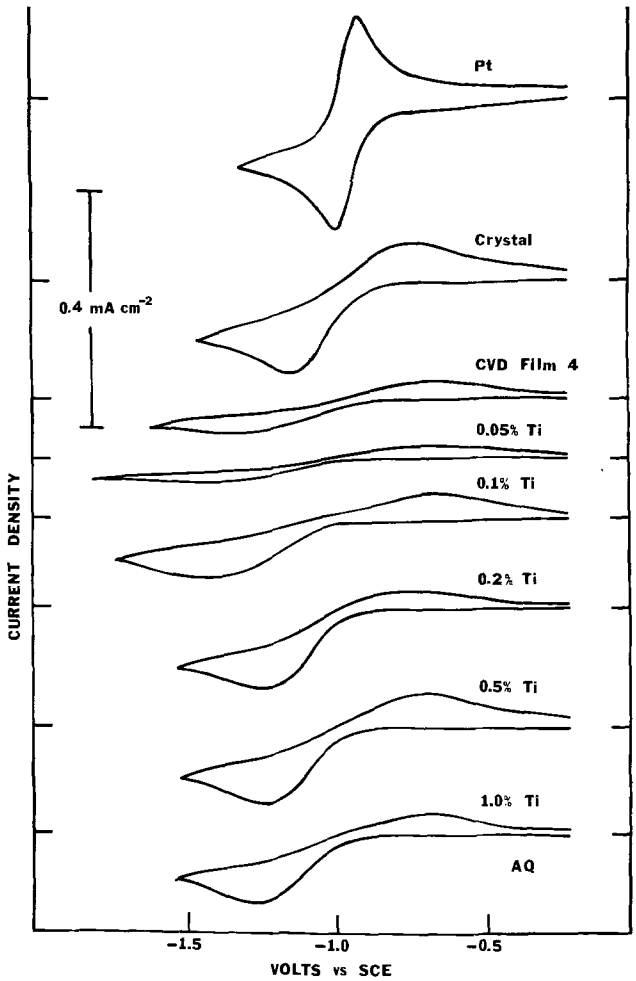

Fig. 4. Cyclic voltammograms of 1.0 mM anthraquinone, 0.100*M* TBAP, ACN, at Fe_2O_3 electrodes at 20 mV sec^{-1}.

with decreasing scan rate and thus the electrodes behave as metals on which the exchange current density is low. Proceeding to couples of higher standard potential, the cyclic voltammograms of oxazine-1 ($Ox\text{-}1^+$) are similar to those of p-benzoquinone (BQ) (Fig. 5) in that the reoxidation is less facile than the initial reduction and the shapes of the anodic peaks are not characteristic of the formation of a diffusion layer near the electrode. The standard potential of the $TMPD^{\cdot +}/TMPD$ couple occurs just positive of the flatband potentials of Fe_2O_3. The cyclic voltammograms (Fig. 6) are very similar for the single crystal and CVD film electrodes but for the sintered polycrystalline electrodes there is a clear trend of increasing anodic current density with increasing Ti content. For the oxidation of 10-MP current densities are small except for the polycrystalline 1.0 a/o Ti electrode unless the electrode is illuminated (Fig. 7). Starting with the cation radical, $10\text{-}MP^{\cdot +}$, only the CVD film and the 0.05 a/o Ti sintered compact fail to give cathodic peaks characteristic of the formation of a diffusion layer. On scan reversal only the 1.0 a/o Ti sintered compact gave an anodic peak. The results for Th and $Ru(bipy)_3^{2+}$ are very similar. Anodic dark current densities are small at potentials <2.0V (SCE) (<20 μA cm^{-2} for single crystal α-Fe_2O_3; <10 μA cm^{-2} for the other electrodes) and cyclic voltammetry, subsequent to oxidation at a platinum foil electrode, yields irreversible reduction waves (Fig. 8).

The cyclic voltammograms reveal that charge transfer processes at Fe_2O_3 are in general slow, as evidenced by a separation, ΔE_p, much larger than that for nernstian behavior (~60 mV). For AQ in ACN at n-ZnO and n-CdS electrodes. ΔE_p has values of 0.11V and 0.19V, respectively, at 200 mV sec^{-1} (26). These

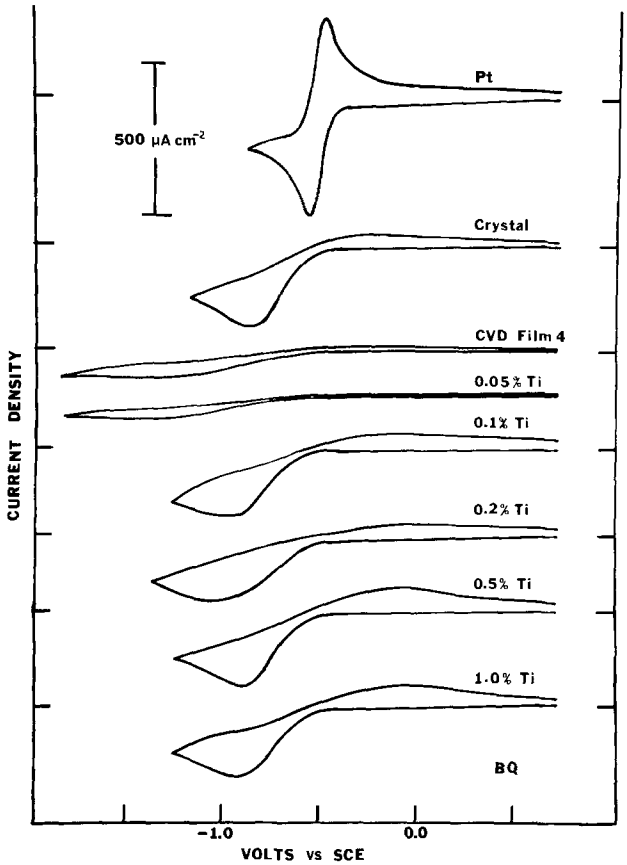

Fig. 5. Cyclic voltammograms of 1.0 mM p-benzoquinone, 0.100M TBAP, ACN, at Fe_2O_3 electrodes at 100 mV sec^{-1}.

contrast with much larger values at Fe_2O_3 (Table II) obtained at a scan rate of 20 mV sec^{-1}. Charge transfer is particularly slow at the CVD film and 0.05 a/o Ti

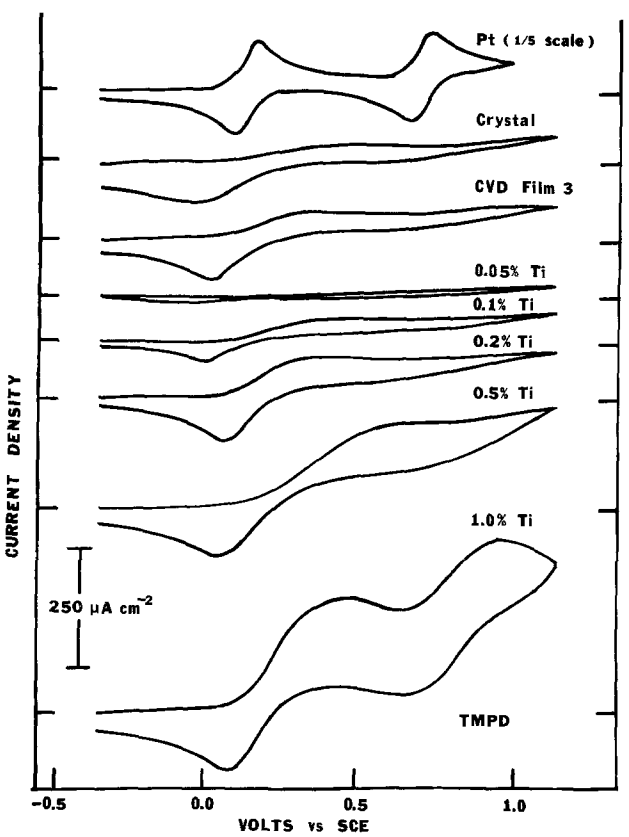

Fig. 6. Cyclic voltammograms of 1.2 mM N,N,N',N'-tetramethyl-p-phenylenediamine, 0.100M TBAP, ACN, at Fe_2O_3 electrodes at 100 mV sec^{-1}.

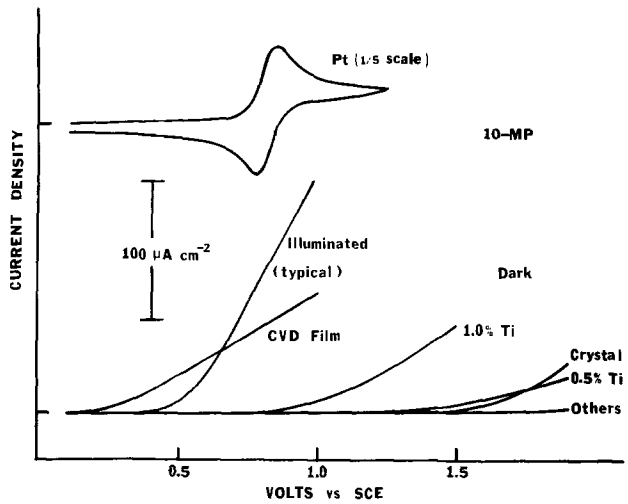

Fig. 7. Linear scan voltammetry of 1.0 mM 10-methylphenothiazine, 0.100M TBAP, ACN, at Fe_2O_3 electrodes and the cyclic voltammogram at a Pt disk all at 50 mV sec^{-1}.

electrodes, although for the former charge transfer appears faster at sample No. 3 than No. 4. Partial rectification is exhibited by the cyclic voltammograms of $Ox\text{-}1^+$ and BQ and rectification becomes more pronounced for couples of higher standard potential and is essentially complete for $Th^{\cdot+}$ and $Ru(bipy)_3^{3+}$ (Fig. 8).

Linear scan voltammetry with chopped illumination. —A typical linear sweep voltammogram with chopped illumination is shown in Fig. 9. At low potentials, but still positive of V_{fb}, illumination causes an anodic current spike decaying with time and on interruption of

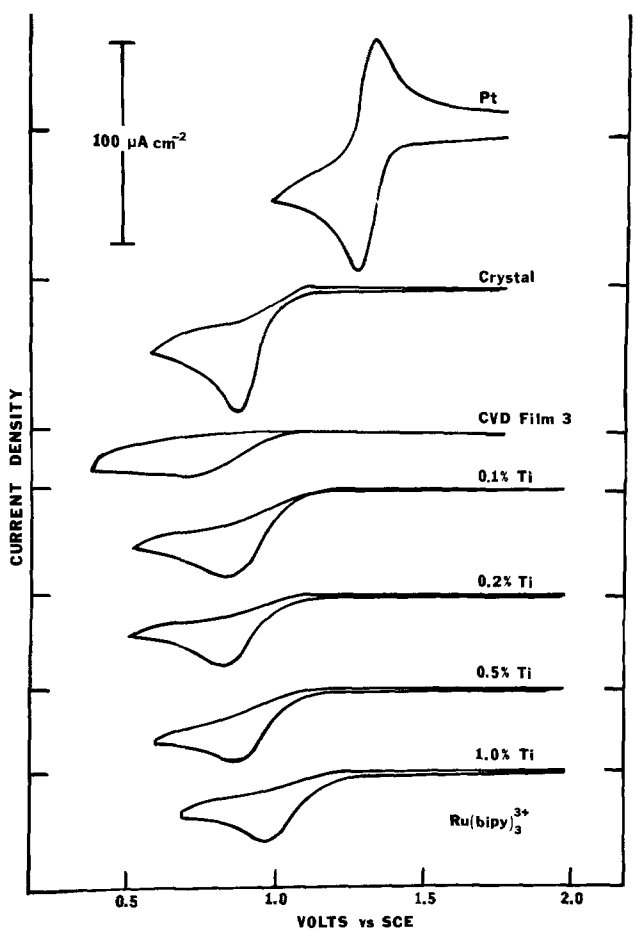

Fig. 8. Cyclic voltammograms of 0.30 mM $Ru(bipy)_3^{3+}$, 0.100M TBAP, ACN, at Fe_2O_3 electrodes at 50 mV sec^{-1}.

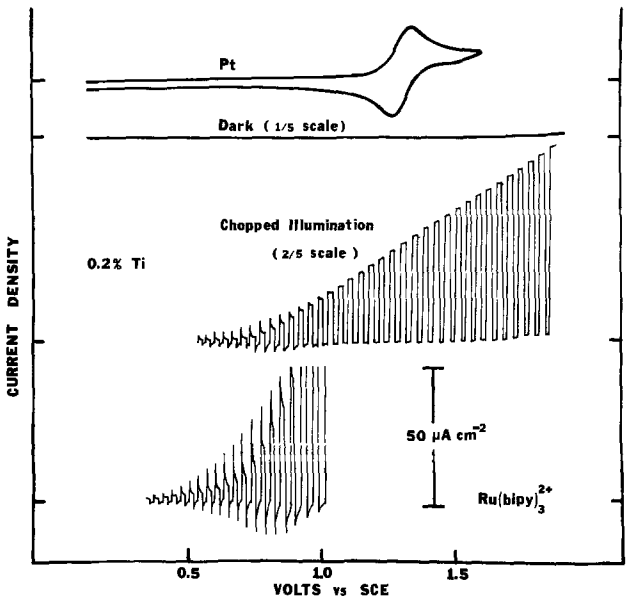

Fig. 9. Linear scan voltammetry in the dark and with chopped illumination of 0.5 mM $Ru(bipy)_3^{2+}$, 0.100M TBAP, ACN, at Fe_2O_3 electrodes at 20 mV sec^{-1} and the cyclic voltammogram at a Pt disk at 50 mV sec^{-1}.

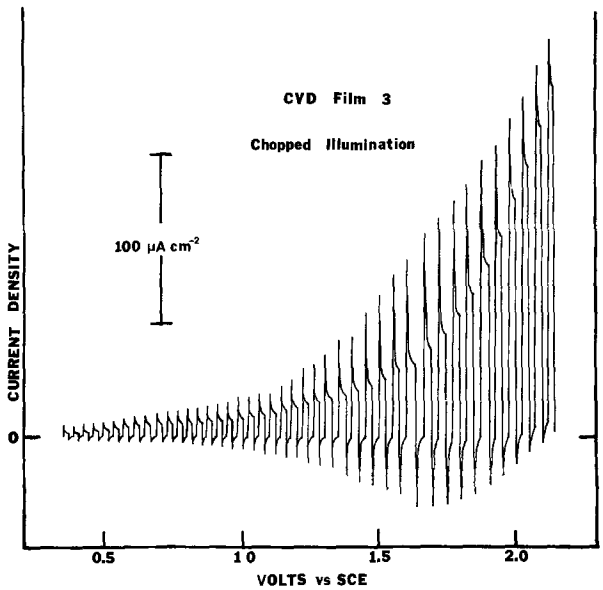

Fig. 10. Linear scan voltammogram with chopped illumination at CVD film 3 in 0.100M TBAP, ACN, at 20 mV sec^{-1}.

the illumination a corresponding cathodic spike results. This behavior has been observed previously (4, 26) and is due to the back (cathodic) reduction of the photo-oxidation product. Scanning to higher potentials causes an increase in the anodic photocurrent and a corresponding increase in the back cathodic current but, while still negative of the reduction peak at platinum, the back reaction ceases. This is manifest by the disappearance of the cathodic current spikes and the spikes on the anodic current peaks. The cathodic current spikes pass through a maximum. Table IV shows the correspondence of these maxima with those of the cyclic voltammograms.

Photo-oxidation of the electrolyte solution also occurs but at photocurrent densities <10% of that in solutions containing 1.0 mM Th. Linear sweep voltammetry with chopped illumination (Fig. 10) exhibits the anodic and cathodic spikes characteristic of the participation of a back cathodic process. The maxima of the cathodic spikes all occur at 1.7-1.9V (SCE) and the effect is most pronounced for the CVD film.

Discussion

Band energy levels.—The results are characteristic of n-type semiconductor electrodes with only anodic photocurrents observed and Schottky-Mott behavior positive of V_{fb}. The data from these experiments (Table II) establish V_{fb} as ~0.0V (SCE) in ACN and, taking the bandgap as 2.2 eV, locates the valence bandedge, E_V, at ~2.2V (SCE) which is the same as

Table IV. Cathodic peak potentials for cyclic voltammetry and chopped illumination linear sweep voltammetry at Fe_2O_3 electrodes

Electrode	E_{pc} (volts, SCE) Th (c.i.[a])	Th+ (c.v.)	$Ru(bipy)_3^{2+}$ (c.i.)	$Ru(bipy)_3^{3+}$
Pt		1.20	—	1.27
Single crystal	0.90	0.83	0.85	0.87
CVD film	0.90	[b]	[b]	[b]
0.1% Ti	0.83	0.87		0.85
0.2% Ti	0.83	0.89	0.82	0.85
0.5% Ti	0.88	0.82	0.83	0.90
1.0% Ti	0.93	0.87	0.89	1.00

[a] Abbreviations: c.i. chopped illumination linear sweep voltammetry; c.v., cyclic voltammetry.
[b] Indistinct peaks.

that found for TiO_2 in ACN (1). The energies of the valence bands of transition metal oxides, formed from oxygen 2p orbitals, are expected to be relatively independent of the transition metal (5).

Band structure and charge transfer.—The standard potentials of $Ox\text{-}1^+/Ox\text{-}1\cdot$ and $BQ/BQ\cdot^-$ lie negative of V_{fb} yet the cyclic voltammograms of $Ox\text{-}1^+$ and BQ exhibit partial rectification. In common with $AQ/AQ\cdot^-$, charge transfer to these couples is slow and the surface becomes nondegenerate (at potentials just negative of V_{fb}) before an overpotential sufficient to produce a diffusion layer is reached. The anodic current is then potential independent.

Gerischer (16) has pointed out that, because charge transfer takes place on a semiconductor near the bandedges where the densities of states are low, charge transfer rates are expected to be slower on semiconductors than on metals. Conduction in n-Fe_2O_3 is by a thermally activated hopping mechanism and Suchet (27) has proposed that for such mechanisms the width of the conduction band is given by $h\nu$ where ν is the frequency of carrier hopping. Morin (10, 11) observed that increasing the dopant concentration from 0.05 to 1.0 a/o Ti increases the carrier mobility by several orders of magnitude. The mobility, μ, is related to the frequency of electron hopping, ν, by

$$\mu = (e\lambda^2\gamma\nu/akT) \exp(-E_A/kT)$$

where a is the lattice constant, λ the diffusion length, γ a geometrical factor, and E_A the activation energy (28). At constant temperature, μ is proportional to ν, and doping with Ti (and presumably other tetravalent metals) may widen the conduction band due to delocalization of the electron states of Fe^{3+} with a concomitant increase in the density of states. This hypothesis provides a possible explanation for the cyclic voltammograms of TMPD. The standard potential of the $TMPD\cdot^+/TMPD$ couple lies just positive of V_{fb} and there must be good overlap of the states of this couple with those of the conduction band. The greater the density of states of the conduction band the greater the exchange current density, i_o. Scanning in the positive direction causes an exponential decrease in the partial cathodic current due to withdrawal of electrons from the surface while the partial anodic current remains essentially constant. Consequently, if i_o is high enough, the net anodic current becomes sufficiently large to produce a diffusion layer. The rates of charge transfer processes occurring at potentials negative of V_{fb} de-

pend exponentially on the potential drop across the Helmholtz layer and the influence of the density of conduction band states is less pronounced.

The oxidation of the electrolyte on Fe_2O_3 electrodes is first detected in the dark at ~1.7V (SCE) (Fig. 3). Except for the CVD film, which is still slightly out of order even when its more negative (by 100 mV) V_{fb} is taken into consideration, there is a trend for electrodes with high N_D to oxidize the electrolyte at lower voltages. This suggests that the thickness of the depletion region is important and that the mechanism involves electron tunneling to the conduction band. Tunneling is possible only through narrow barriers and, at potentials near E_v, the depletion region may be contracted by the ionization of deep donors or the neutralization of acceptors. Divalent cation impurities (*e.g.*, Cu^{2+}, Zn^{2+}, and Mg^{2+}) are known acceptors in Fe_2O_3 (29) and it has been found that small additions of TiO_2 usually decrease the conductivity due to the neutralization of these impurity acceptors (14).

Surface states.—If, at potentials well positive of V_{fb}, the semiconductor/electrolyte solution interface formed a true Schottky barrier charge transfer at such potentials should be negligibly slow in both directions. However, cathodic spikes are observed in the chopped illumination linear scan voltammograms of Th and $Ru(bipy)_3^{2+}$ (Fig. 9) and $Th^{\cdot+}$ and $Ru(bipy)_3^{3+}$ are reduced directly (Fig. 8). Table IV shows the correspondence between these peaks. Since these reductions occur deep in the bandgap [~0.85V (SCE)] and, since electron transfer is isoenergetic, surface states must mediate the transfer of charge. In keeping with previous observations (26) of n-type semiconductors, surface states do not mediate anodic processes. This has been interpreted as due to the presence of an energy barrier for electron transfer from surface states to the conduction band (26). The peaks in the cathodic spikes of the chopped illumination linear scan voltammograms of the electrolyte solution at 1.7-1.9V (SCE) (Fig. 10) results from a sudden decrease but not cessation of the back reaction. This is evidenced by the continuation of spikes on the anodic side and thus the peak cannot be due to the Fermi level dropping below the reversible potential for the reduction of $ClO_2^{\cdot}$. The most probable explanation is the Fermi level passing through surface states and the residual back reaction is then caused by overlap with the valence band and hole injection into it. These results establish that surface states capable of mediating charge transfer have density maxima at ~ 0.9 and ~ 1.8 eV negative of the conduction band-edge.

The more positive the standard potential of a redox couple, the better the overlap of the energy levels of the reductant with the valence band and higher efficiencies for photo-oxidations are expected. In the present work, the photocurrent for the oxidation of TMPD is detected at lower potentials than those for the oxidation of Th or $Ru(bipy)_3^{2+}$. This is because the energy levels of the photo-oxidation products of the latter species $Th^{\cdot+}$ and $Ru(bipy)_3^{3+}$ overlap well with the surface states at ~0.9V (SCE) and at more negative potentials the net anodic photocurrent is diminished by the cathodic back reaction. The onset of the photocurrent is then more difficult to detect.

Acknowledgment

The support of this work by the National Science Foundation is gratefully acknowledged.

Manuscript submitted Jan. 22, 1979; revised manuscript received May 8, 1979.

Any discussion of this paper will appear in a Discussion Section to be published in the June 1980 JOURNAL. All discussions for the June 1980 Discussion Section should be submitted by Feb. 1, 1980.

Publication costs of this article were assisted by The University of Texas at Austin.

REFERENCES

1. K. L. Hardee and A. J. Bard, *This Journal*, **123**, 1024 (1976).
2. R. K. Quinn, R. D. Nasby, and R. J. Baugham, *Mater. Res. Bull.*, **11**, 1011 (1976).
3. J. H. Kennedy and K. W. Frese, Jr., *This Journal*, **125**, 709 (1978).
4. K. L. Hardee and A. J. Bard, *ibid.*, **124**, 215 (1977).
5. H. H. Kung, H. S. Jarrett, A. W. Sleight, and A. Ferretti, *J. Appl. Phys.*, **48**, 2463 (1977).
6. J. H. Kennedy and K. W. Frese, Jr., *This Journal*, **125**, 723 (1978).
7. R. N. Noufi, Dissertation, University of Texas, Austin, Texas (1978).
8. R. F. G. Gardner, F. Sweett, and D. W. Tanner, *J. Phys. Chem. Solids*, **24**, 1183 (1963).
9. R. F. G. Gardner, R. L. Moss, and D. W. Tanner, *Br. J. Appl. Phys.*, **17**, 55 (1966).
10. F. J. Morin, *Phys. Rev.*, **83**, 1005 (1951).
11. F. S. Morin, *ibid.*, **93**, 1195 (1954).
12. H. J. van Daal and A. J. Bosman, *ibid.*, **158**, 736 (1967).
13. D. Adler, in "Solid State Physics," Vol. 21, F. Seitz, D. Turnbull, and H. Ehrenreich, Editors, pp. 79-83, Academic Press, New York (1968).
14. J. B. Goodenough, in "Progress in Solid State Chemistry," Vol. 5, H. Reiss, Editor, pp. 298-301, Pergamon Press, New York (1969).
15. J. P. Suchet, "Crystal Chemistry and Semiconduction in Transition Metal Binary Compounds," pp. 184-190, Academic Press, New York (1971).
16. H. Gerischer, in "Adv. Electrochem. Electrochem. Eng.," Vol. 1, P. Delahay, Editor, Chap. 4, Interscience Pub., New York (1961).
17. H. Gerischer, in "Physical Chemistry—An Advanced Treatise," Vol. 9A, H. Eyring, D. Henderson, and W. Jost, Editors, Chap. 5, Academic Press, New York (1970).
18. S. N. Frank, and A. J. Bard, *J. Am. Chem. Soc.*, **97**, 7427 (1975).
19. D. Laser and A. J. Bard, *J. Phys. Chem.*, **80**, 459 (1976).
20. S. N. Frank, A. J. Bard, and A. Ledwith, *This Journal*, **122**, 898 (1975).
21. F. Cardon and W. P. Gomes, *J. Phys. D.*, **11**, L63 (1978).
22. W. H. Laflere, R. L. Van Meirhaeghe, F. Cardon, and W. P. Gomes, *Surf. Sci.*, **59**, 401 (1976).
23. V. A. Myamlin and Y. V. Pleskov, "Electrochemistry of Semiconductors," Chap. 3, Plenum Press, New York (1967).
24. P. Merchant, R. Collins, R. Kershaw, K. Dwight, and A. Wold, Private communication (1978).
25. J. N. Hodgson, "Optical Absorption and Dispersion in Solids," Chap. 3, Chapman and Hall, London (1970).
26. P. A. Kohl and A. J. Bard, *J. Am. Chem. Soc.*, **99**, 7531 (1977).
27. J. P. Suchet, "Crystal Chemistry and Semiconduction in Transition Metal Binary Compounds," p. 66, Academic Press, New York (1971).
28. R. R. Heikes and D. W. Johnston, *J. Chem. Phys.*, **26**, 582 (1957).
29. R. F. G. Gardner, F. Sweett, and D. W. Tanner, *J. Phys. Chem. Solids*, **24**, 1175 (1963).